Hyperfine Interactions (2020) 241: 31
https://doi.org/10.1007/s10751-019-1654-z

Synthesis and characterization of copper-nickel ferrite catalysts for ethyl acetate oxidation

Nikolay Velinov[1] · Tanya Petrova[1] · Radostina Ivanova[2] · Tanya Tsoncheva[2] · Daniela Kovacheva[3] · Ivan Mitov[1]

Published online: 25 February 2020

Abstract
Materials with nominal composition $Cu_{0.5}Ni_{0.5}Fe_2O_4$ were prepared by sol-gel auto-combustion technique using corresponding metal nitrates and citric acid as complexating agent/fuel agent. Different ratios between citric acid and metal ions were used to control the combustion reaction. For comparison, $Cu_{0.5}Ni_{0.5}Fe_2O_4$ ferrite was also synthesised by co-precipitation. Mössbauer spectroscopy was used for analysis of synthesised samples both at room temperature and liquid nitrogen boiling temperature. Iron distribution in tetrahedral and octahedral positions of spinel lattice was determined. Different degrees of agglomeration of the ferrite phase were estimated by super-paramagnetic behaviour of samples. In addition, methods of X-Ray Diffraction, UV-Vis, FTIR, nitrogen physisorption, TPR with hydrogen were applied for structural characterization of the materials. Some quantities of secondary phases (Cu, Cu-Ni alloy and hematite) were found out in samples prepared by auto-combustion method. The catalytic activities of the samples in ethyl acetate oxidation reaction strongly depended on the variations in the structural and texture characteristics of the samples. The sample synthesized at the highest ratio of citric acid to metal ions is characterized by the smallest ferrite crystallite size, the higher surface area and the best catalytic activity.

Keywords Copper-nickel ferrites · Mössbauer spectroscopy · Auto-combustion sol-gel method · Catalysis · Ethyl acetate oxidation

This article is part of the Topical Collection on *Proceedings of the International Conference on the Applications of the Mössbauer Effect (ICAME2019)*, 1-6 September 2019, Dalian, China
Edited by Tao Zhang, Junhu Wang and Xiaodong Wang

✉ Nikolay Velinov
nikivelinov@ic.bas.bg

[1] Institute of Catalysis, Bulgarian Academy of Sciences, Acad. G. Bonchev str., bl.11, 1113 Sofia, Bulgaria

[2] Institute of Organic Chemistry with Centre of Phytochemistry, Bulgarian Academy of Sciences, Acad. G. Bonchev str., bl.9, 1113 Sofia, Bulgaria

[3] Institute of General and Inorganic Chemistry, Bulgarian Academy of Sciences, Acad. G. Bonchev str., bl.11, 1113 Sofia, Bulgaria

1 Introduction

Spinel ferrites with general formula $(Me_xFe_{1-x})_{tetra}[Me_yFe_{2-y}]_{octa}O_4$, where Me is divalent metal ion have been recently the subject of many studies because of their structure dependent properties [1, 2]. Cation distribution in lattice could be varied by mixing two or more different divalent ions or by varying nature of the ions, and therefore properties as magnetic [3–5], electric [6–9] and catalytic materials [10–15] could be tuned. Spinel ferrites with different structural characteristics can be synthesized using different methods of synthesis or varying conditions of preparation [16]. The auto-combustion sol-gel method has been successfully applied for various spinel ferrite materials synthesis [17–20]. In a previous study, it has been established that ferrite materials with different crystallite sizes and different catalytic activities in reaction of methanol decomposition can be obtained by auto-combustion synthesis varying pH of the initial solution [21]. By varying synthesis conditions including complexating agent, concentration, oxygen balance etc., it has become possible to control system stability, xerogel microstructure, reaction temperature and rate and volume of gases generated. This influences the crystallite size, defect sites concentration, particles agglomeration, thus affecting properties of produced materials [16].

The aim of present work was to obtain $Cu_{0.5}Ni_{0.5}Fe_2O_4$ ferrite materials with different structural characteristics and to study their behaviour in catalytic volatile organic compounds (VOCs) removal.

2 Experimental

Samples with nominal composition $Cu_{0.5}Ni_{0.5}Fe_2O_4$ were synthesized by auto-combustion sol-gel method [13] at different ratios of the sum of the metal ions to citric acid. Shortly, the experimental procedure was as follows: $Cu(NO_3)_2.3H_2O$, $Ni(NO_3)_2.6H_2O$ and $Fe(NO_3)_3.9H_2O$ in corresponding stoichiometric ratio were dissolved in distilled water at room temperature under stirring; citric acid was added to the solution and stirring was continued at 333 K; the auto-combustion process was performed by heating the samples in an oven at 423 K for two hours. The samples were further thermally treated at 573 K for two hours. The samples were designated as CAx, where x is the ratio of citric acid to the sum of the metal ions. For comparison, one sample having nominal composition $Cu_{0.5}Ni_{0.5}Fe_2O_4$ was synthesised by co-precipitation method [22]. The mixed nitrate solution containing metal cations of Cu, Ni, Fe in molar ratio was precipitated with dropwise addition of 1 M sodium carbonate up to pH 9 during continuous stirring. The obtained precipitate was washed with distilled water until absence of nitrates and dried up at 323 K for 24 h to form precursor powder. Finally, the sample was obtained by heat treatment of the precursor powder at 773 K for 2 h and it was denoted as HC.

Powder X-ray diffraction (XRD) patterns were collected within the range of 15° to 80° 2θ on a Bruker D8 Advance diffractometer with Cu K_α radiation and LynxEye detector. Phase identification was performed using ICDD-PDF2 Database. The average crystallite size (D), and the lattice parameters (a, c) of the crystalline phases in the samples were determined based on the experimental XRD profiles by using the PowderCell-2.4 software and appropriate corrections for the instrumental broadening.

The Mössbauer spectra were obtained in air at room temperature (RT) and liquid nitrogen boiling temperature (LNT) with a Wissel (Wissenschaftliche Elektronik GmbH, Germany)

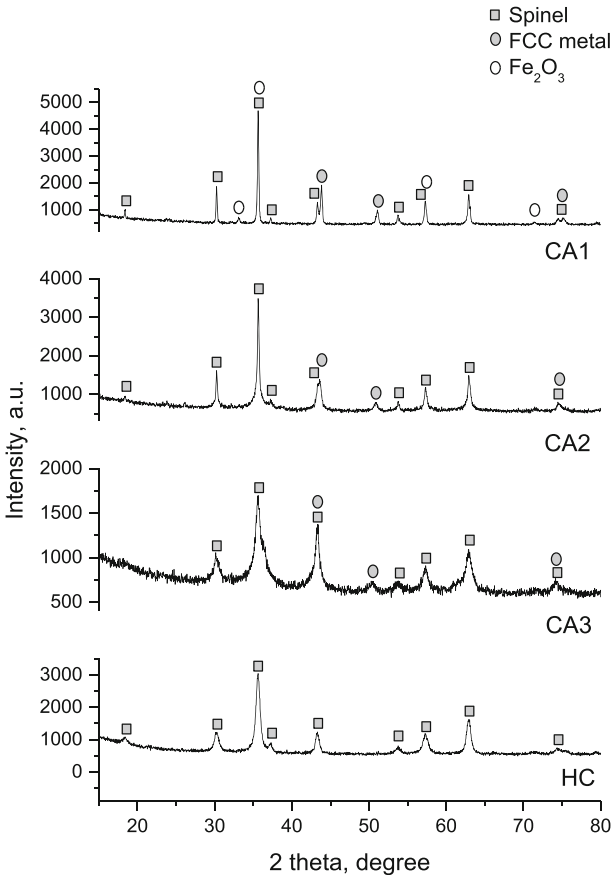

Fig. 1 XRD patterns of the investigated samples

electromechanical spectrometer working in a constant acceleration mode. A ^{57}Co/Rh (activity ≅ 50 mCi) source and α-Fe standard were used. The experimentally obtained spectra were fitted using CONFIT2000 software [23]. The parameters of hyperfine interaction such as isomeric shift (δ), quadrupole splitting (Δ), quadrupole shift (2ε), magnetic hyperfine field

Table 1 Average crystallite size (D) and lattice parameters (a, c) of the crystalline phases in samples determined based on the experimental XRD profiles

Sample	Phase	D, nm	*a (c)*, Å	%
HC	Spinel	14.92	8.34	100
CA3	Spinel	9.65	8.37	94
	Cu	33.48	3.63	6
CA2	Spinel	41.50	8.36	90
	Cu-Ni-alloy	22.21	3.60	10
CA1	Spinel	146.75	8.35	76
	a-Fe_2O_3	21.97	a=5.04	13
			c=13.75	
	Cu-Ni-alloy	45.38	3.57	11

(B_{hf}), line widths (Γ_{exp}), and relative weight (G) of the partial components in the spectra were determined.

The UV–Vis spectra were collected on a Jasco V-650 UV-Vis spectrophotometer. FTIR spectra were recorded on a Bruker Vector 22 spectrometer at a resolution of 1–2 cm^{-1}, accumulating 64–128 scans using KBr pellets technique. The textural characteristics were measured from the Nitrogen adsorption/desorption isotherms obtained at 77 K using Quantachrome Instruments NOVA 1200e (USA). Prior to the measurements, the samples were outgassed for 2 h at 200 °C under vacuum. The nitrogen adsorption-desorption isotherms were analyzed to evaluate the following parameters: the specific surface areas (S_{BET}) were determined on the basis of the BET equation, the total pore volume (V_t) and average pore diameter (D_{av}) were estimated according to the rule of Gurvich at a relative pressure being close to 0.99.

The TPR/TG (temperature-programmed reduction/thermo-gravimetric) analyses were performed on a Setaram TG92 instrument in 100 cm^3 min^{-1} flow of H_2 in Ar (volume ratio of 1) and heating rate of 5 K min^{-1}.

The total oxidation of ethyl acetate was performed under temperature programmed regime within the range of 400–773 K in a flow of 1.21 mol% ethyl acetate in air with WHSV of 100 h^{-1}. Gas chromatographic analyses were carried out on a HP 5890 apparatus using carbon-based calibration.

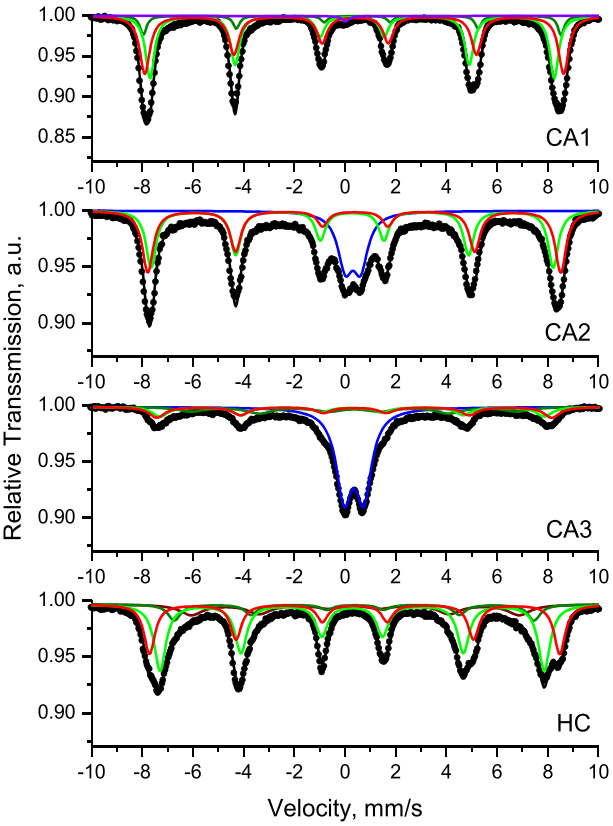

Fig. 2 Mössbauer spectra at room temperature of the synthesized samples

Table 2 Mössbauer parameters of the synthesized samples at room temperature and liquid nitrogen boiling temperature (LNT)

Sample	Components	δ, mm/s	$\Delta(2\varepsilon)$, mm/s	B_{hf}, T	Γ_{exp}, mm/s	G, %
HC	Sx1-Fe^{3+}_{octa}	0.38	-0.01	50.3	0.52	29
	Sx2-Fe^{3+}_{tetra}	0.28	0.00	47.1	0.56	46
	Sx3-Fe^{3+}_{octa}	0.38	-0.04	44.1	0.60	11
	Sx4-Fe^{3+}_{octa}	0.38	0.04	40.2	1.07	14
CA3	Sx1-Fe^{3+}_{octa}	0.38	-0.02	48.4	0.75	16
	Sx2-Fe^{3+}_{tetra}	0.28	0.00	47.1	0.75	15
	Sx3-Fe^{3+}	0.35	0.00	40.0	1.20	15
	Db-Fe^{3+}	0.35	0.78	-	0.76	54
CA3 LNT	Sx1-Fe^{3+}_{octa}	0.47	0.01	52.8	0.47	17
	Sx2-Fe^{3+}_{tetra}	0.40	0.00	50.5	0.63	25
	Sx3-Fe^{3+}	0.46	-0.03	44.8	1.48	42
	Db-Fe^{3+}	0.47	0.92	-	0.70	16
CA2	Sx1-Fe^{3+}_{octa}	0.38	-0.04	50.6	0.52	28
	Sx2-Fe^{3+}_{tetra}	0.28	0.00	49.3	0.48	29
	Sx3-Fe^{3+}	0.39	0.07	43.4	1.83	26
	Db-Fe^{3+}	0.31	0.60	-	0.71	17
CA1	Sx1-Fe^{3+}_{octa}	0.38	-0.04	51.3	0.47	47
	Sx2-Fe^{3+}_{tetra}	0.28	0.00	50.0	0.42	43
	Sx3-α-Fe_2O_3	0.38	-0.20	51.2	0.30	9
	Sn-Fe^0	0.02	-	-	0.30	1

3 Results and discussion

The XRD patterns of synthesized samples are represented in Fig. 1. Cubic spinel phase (S.G. Fd3m, No. 227) is found out in all the samples. Average crystallite size and lattice parameter of phases in the samples determined on the basis of the experimental XRD profiles are represented in Table 1. Decreasing the ratio of citric acid to metal ions in the gel leads to increase of quantity of secondary phases and significantly increasing of spinel crystallite size. This could be explained by increase in the temperature of combustion upon decreasing the relative part of citric acid in the gel. Metallic FCC phases are formed as impurities in all CA samples under the

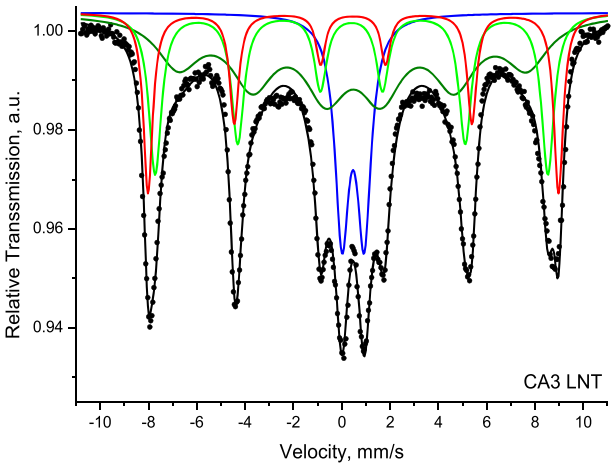

Fig. 3 Mössbauer spectrum of sample CA3 at liquid nitrogen boiling temperature

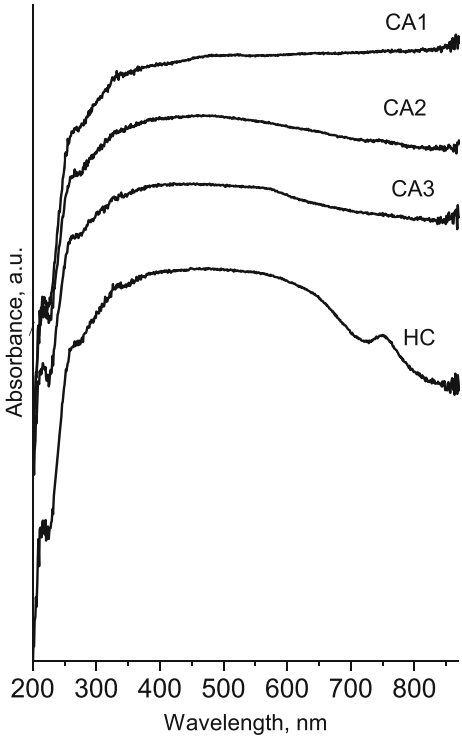

Fig. 4 UV–Vis spectra of the synthesized samples

reductive atmosphere during the combustion. The lattice parameter of the metallic phase in sample CA3 corresponds to copper (Table 1). A permanent decrease in the lattice parameters of metallic phase upon decreasing of the x ratio is observed indicating formation of Cu-Ni alloys with a tendency of increase in nickel content inside them upon decreasing the amount of citric acid in the gel. Additionally, hematite is found out in CA1 sample, which proves that lower complexating agent content in gel leads to formation of more inhomogeneous sample. For comparison, pure ferrite phase with average crystallite size of 15 nm is detected for the sample obtained by traditional sol-gel method.

Mössbauer spectra of the synthesized samples recorded at room temperature are represented in Fig. 2. The spectra are consisting of sextet components with typical parameters for Fe^{3+} in octahedral coordination ($\delta = 0.38$ mm/s) and Fe^{3+} in tetrahedral coordination ($\delta = 0.28$ mm/s) in spinel phases, as well as broad sextets with lower hyperfine field and doublets. Calculated hyperfine parameters are represented in Table 2. A Mössbauer spectrum of CA3 at liquid nitrogen boiling temperature (LNT) was recorded in order to clarify the doublet nature (Fig. 3, Table 2). The relative weight of doublet is 16% at LNT comparing with 54% at room temperature. This evidences contribution of spinel particles with paramagnetic behaviour in the doublets in the CA2 and CA3 spectra. Therefore, the broadened sextets with lower field could be assigned to spinel particles with middle size i.e. larger than particles with paramagnetic behaviour and smaller than the well crystallized spinel particles characterized with Sx1 and Sx2. The presence of superparamagnetic particles in CA2 and CA3 samples are well correlated to the results for average crystallite size, calculated from XRD (Table 1). It is interesting that the average crystallites size of spinel phase in HC sample lies in between those of CA2 and CA3, but in Mössbauer spectrum superparamagnetic doublet is not observed. This

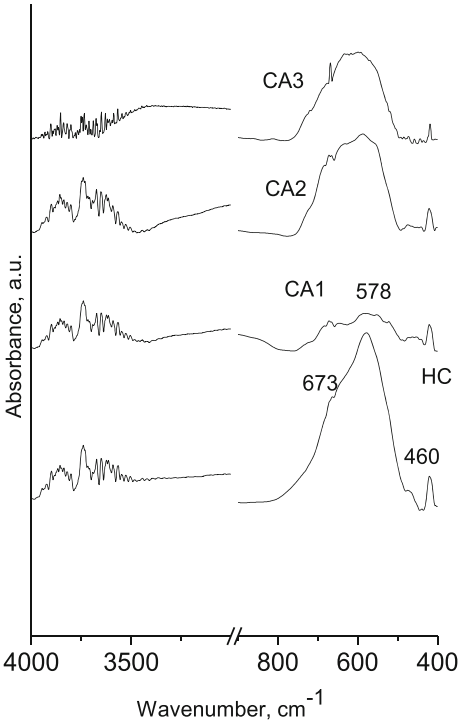

Fig. 5 FTIR spectra of the synthesized samples

could be explained by narrower particles size distribution in the sample prepared by co-precipitation compared to samples prepared by auto-combustion methods. The singlet in CA1 spectrum has nearly zero isomeric shift and relative weight about 1% and it is probably due to iron atoms incorporated in FCC Cu-Ni alloy, which is detected by XRD (Table 1).

UV–Vis diffuse reflectance spectra were collected to study the optical properties of the synthesized ferrates (Fig. 4). The appearance of continuous strong absorption band above 300 nm indicates the formation of ferrite phase. The variation in the absorption bands of the materials obtained under different preparation conditions could be due to the difference in their composition and physicochemical properties, such as particle size for example [24]. Thus, the observed decrease in the absorption with a simultaneous shift of the bands to lower wavelength upon decreasing the citric acid contents in the gel could be assigned to the formation of ferrite phase with larger crystallites and high degree of impurity and this is in good correlation with the XRD and Mössbauer data.

Table 3 Nitrogen physisorption data: S_{BET} - specific surface area, V_t - total pore volume, D_{av} – average pore diameter of the synthesized samples

Sample	S_{BET} [m^2/g]	V_t [cm^3/g]	D_{av} [nm]
HC	37	0.14	14.8
CA3	92	0.21	9.1
CA2	58	0.09	6.1
CA1	1	0.00	15.8

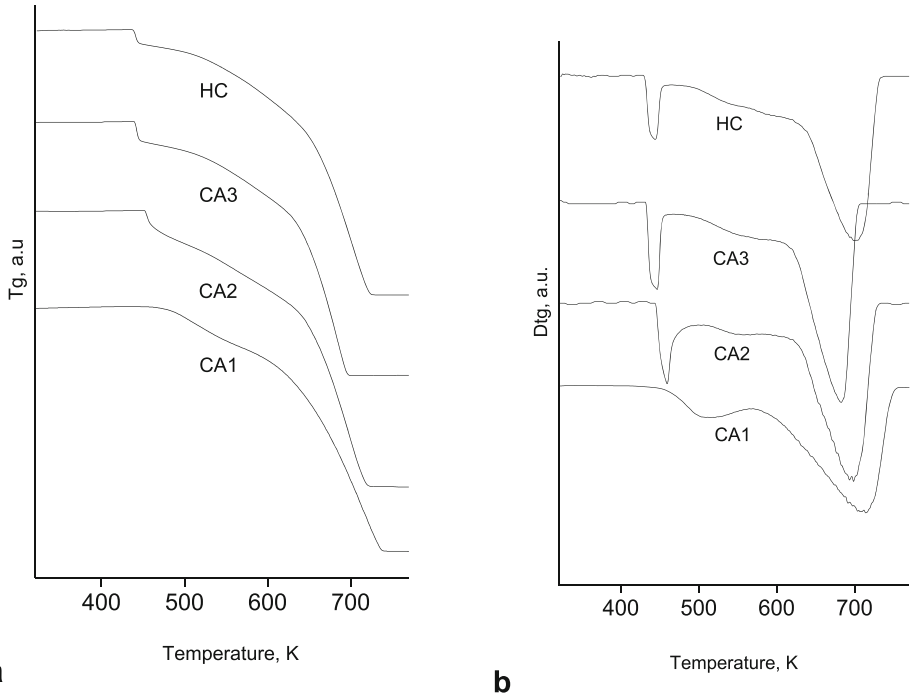

Fig. 6 H_2-TPR of the synthesized materials: TG (a) and DTG (b) curves

Figure 5 represents FTIR spectra of all the synthesized materials. The spectra illustrate strong absorption bands at 570–590 cm^{-1}, which could be assigned to M-O stretching vibration of metal ions in tetrahedral position in the spinel. The bands at around 460 cm^{-1} are usually assigned to the vibrations of M-O bonds in octahedral sites. The shift of the bands of M-O bonds in tetrahedral sites to higher frequencies, accompanied by a decrease in the absorption bands at around 460 cm^{-1} with the increase of the *x* ratio, could be an indication for a decrease in the ratio of Cu^{2+} ions in the spinel. According to ref. [25] this could be due to the migration of Fe^{3+} ions from octahedral to tetrahedral position as a result of segregation of Cu or Cu rich alloys as it was also assumed from the XRD data (Table 1). The shoulder at around 670 cm^{-1} and the small bands at circa 430 cm^{-1} could be due to the formation of regions with local structural ordering identical to that of pure $NiFe_2O_4$ [26]. The absorption bands at 3500 cm^{-1} are typically assigned to stretching vibrations of O-H bods in adsorbed water molecules.

The textural characteristics of samples were evaluated by nitrogen physisorption. The results from these measurements are summarized in Table 3. The values of the specific surface area are within the range from 1 to 92 m^2/g. Clear tendency of specific surface area increase and pore volume decrease upon increasing the citric acid concentration is observed. This is probably related to the improved dispersion of the samples and this is in consistence with the XRD (Table 1) and Mössbauer (Table 2) data.

In Fig. 6 the TPR profiles in hydrogen in the 300–750 K range are shown. The TG curves (Fig. 6a) display continuous weight loss at temperature above 400 K, which is due to reduction transformation of the samples. The low-temperature effect at about 450–470 K could be assigned to the reduction of Cu^{2+} to metallic copper, while the weight loss within the 500–

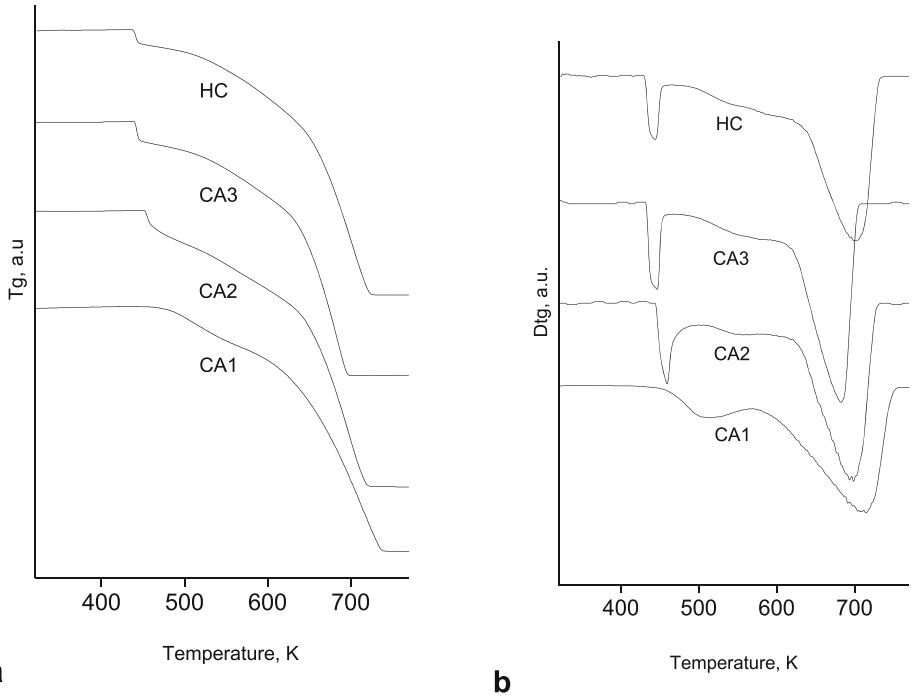

Fig. 7 Ethyl acetate conversion degree vs catalyst bed temperature and specific surface area at 550 K (inset) for various samples

600 K range is probably due to superposition of reduction transformations of Ni^{2+} to metallic Ni and Fe^{3+} to $Fe^{2.5+}$ [27] . The main effect centered at 680–700 K is due to the reduction of Fe_3O_4 into metallic Fe. The broadening of the TPR effects combined with their shift to higher temperature with the decrease in the citric acid content in the gel indicate presence of more non-homogeneous and slightly-dispersed phase and this is in consistence with the XRD and spectroscopic data.

Figure 7 represents the temperature dependencies of ethyl acetate oxidation reaction. The samples demonstrate catalytic activity above 500–570 K. For all materials 80–100% selectivity to CO_2 is achieved at 600 K, while ethanol, acetaldehyde and acetic acid in different proportion are detected as by-products at lower temperature. According to the shift in the conversion curves towards the temperature axis, the catalytic activities of the samples are decreasing in the following order: CA3 > CA2 > HC > CA1. It correlates well with the decrease in the specific surface area (Fig. 7 inset), determined by the decrease in the dispersion (Tables 1, 2), which is controlled by the preparation procedure used. Moreover, the main catalytic activity contribution of $Cu_{0.5}Ni_{0.5}Fe_2O_4$ phase in ethyl acetate oxidation and negligible effect of metals impurities could be assumed. Mössbauer spectra of catalysts after the catalytic activity test were measured to evaluate the materials stability (Fig. 8, Table 4). The absence of any phase transformation with the samples evidences their stability under the reaction medium conditions. The observed small decrease in the doublet part in the CA2 and CA3 spectra on behalf of the sextet part increase after catalysis is probably due to partial recrystallization of superparamagnetic spinel particles. Obviously, the use of auto-combustion method with high citric acid to metal ions ratio in the gel leads to preparation of more homogeneous and finely

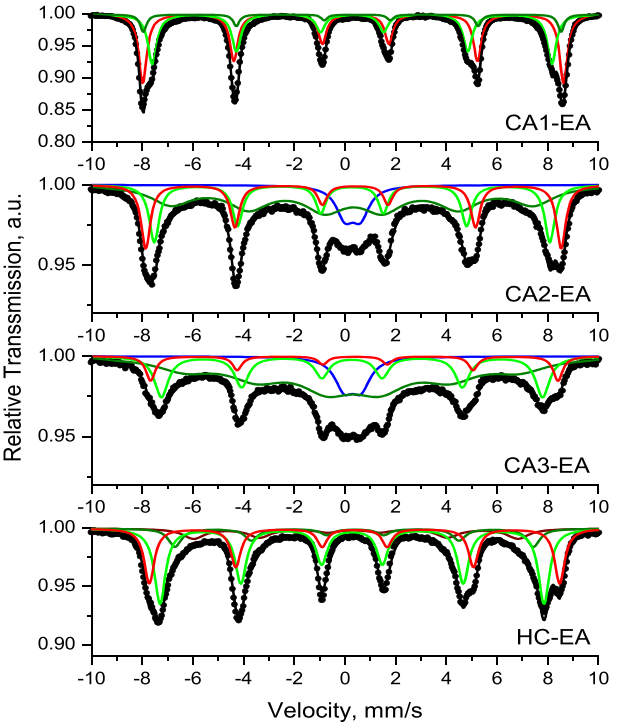

Fig. 8 Mössbauer spectra at room temperature of samples after catalytic activity test in ethyl acetate oxidation reaction

dispersed $Cu_{0.5}Ni_{0.5}Fe_2O_4$ phase, which ensures high catalytic activity and stability in ethyl acetate oxidation.

Table 4 Mössbauer parameters of the synthesized samples after catalytic activity test in ethyl acetate oxidation reaction

Sample	Components	δ, mm/s	$\Delta(2\varepsilon)$, mm/s	B_{hf}, T	Γ_{exp}, mm/s	G, %
HC-EA	Sx1-Fe^{3+}_{octa}	0.38	0.00	50.3	0.48	29
	Sx2-Fe^{3+}_{tetra}	0.28	0.00	47.1	0.53	47
	Sx3-Fe^{3+}_{octa}	0.38	-0.04	43.9	0.62	12
	Sx4-Fe^{3+}_{octa}	0.38	0.09	40.0	1.03	12
CA3-EA	Sx1-Fe^{3+}_{octa}	0.38	-0.03	49.9	0.44	8
	Sx2-Fe^{3+}_{tetra}	0.27	0.00	46.7	0.66	24
	Sx3-Fe^{3+}	0.31	-0.04	41.0	2.63	58
	Db-Fe^{3+}	0.30	0.66	-	0.90	10
CA2-EA	Sx1-Fe^{3+}_{octa}	0.37	-0.07	50.9	0.44	21
	Sx2-Fe^{3+}_{tetra}	0.28	0.00	48.5	0.48	23
	Sx3-Fe^{3+}	0.31	-0.05	44.4	1.95	47
	Db-Fe^{3+}	0.30	0.62	-	0.83	9
CA1-EA	Sx1-Fe^{3+}_{octa}	0.37	-0.10	51.6	0.38	51
	Sx2-Fe^{3+}_{tetra}	0.28	0.00	49.0	0.42	40
	Sx3-α-Fe_2O_3	0.38	-0.20	51.2	0.30	9

4 Conclusions

Materials with nominal composition $Cu_{0.5}Ni_{0.5}Fe_2O_4$ and different structural characteristics were prepared by sol-gel auto-combustion technique varying the ratio between citric acid and metal nitrates. Cubic spinel phase was found out in all the samples. The citric acid to metal ions ratio decrease leads to significant increase in spinel crystallite size and formation of secondary phases. The catalytic activities of the samples in ethyl acetate oxidation are strongly dependent on the variations in the texture and structure characteristics of the samples. The increase in the citric acid content in the gel provides the preparation of highly dispersed ferrite phase, with high specific surface area, improved redox properties and excellent catalytic activity in total oxidation reaction of ethyl acetate.

Acknowledgements This work was supported by the Bulgarian Science Fund (Contract No. КП-06-Н29/2/ 2018). T. Tsoncheva also thanks Project BG05M2OP001-1.002-0019: „Clean technologies for sustainable environment – water, waste, energy for circular economy"(Clean&Circle), for development of a Centre of Competence.

References

1. Mahmoud, M., Hassan, A.M., Ahmed, M.A., Kaixin, Z., Ganeshraja, A.S., Wang, J.: Mössbauer and magnetic studies of nanocrystalline zinc ferrites synthesized by microwave combustion method. Hyperfine Interact. **237**(17), 1–11 (2016)
2. Verma, V., Kaur, M., Greneche, J.M.: Tailored structural, optical and magnetic properties of ternary nanohybrid $Mn_{0.4}Co_{0.6-x}Cu_xFe_2O_4$ (x= 0, 0.2, 0.4, 0.6) spinel ferrites. Ceram. Int. **45**(8), 10865–10875 (2019)
3. Subramani, A.K., Kondo, K., Tada, M., Abe, M., Yoshimura, M., Matsushita, N.: Spinel ferrite films by a novel solution process for high frequency applications. Mater. Chem. Phys. **123**, 16–19 (2010)
4. Motavallian, P., Abasht, B., Mirzaee, O., Abdollah-Pour, H.: Correlation between structural and magnetic properties of substituted (cd, Zr) cobalt ferrite nanoparticles. Chin. J. Phys. **57**, 6–13 (2019)
5. Muscas, G., Jovanović, S., Vukomanović, M., Spreitzer, M., Peddis, D.: Zn-doped cobalt ferrite: tuning the interactions by chemical composition. J. Alloys Compd. **796**, 203–209 (2019)
6. Bagade, A.A., Rajpure, K.Y.: Studies on NO_2 gas sensing properties of sprayed $Co_{1-x}Mn_xFe_2O_4$ ($0 \le x \le 0.5$) spinel ferrite thin films. Ceram. Int. **41**, 7394–7401 (2015)
7. Kumbhar, V.S., Jagadale, A.D., Shinde, N.M., Lokhande, C.D.: Chemical synthesis of spinel cobalt ferrite ($CoFe_2O_4$) nano-flakes for supercapacitor application. Appl. Surf. Sci. **259**, 39–43 (2012)
8. Sharif, M., Jacob, J., Javed, M., Manzoor, A., Mahmood, K., Khan, M.A.: Impact of co and Mn substitution on structural and dielectric properties of lithium soft ferrites. Phys. B Condens. Matter. **567**, 45–50 (2019)
9. Ansari, M., Khan, S., Ahmad, N.: A comprehensive investigation of structural, thermal and electrical properties of $T_{0.35}Zn_{0.55}Cu_{0.1}Fe_2O_4$ (T = Mn, Ni) nano ferrites. Physica B: Condensed Matter. **566**, 86–95 (2019)
10. Wang, Y., Zhao, H., Li, M., Fan, J., Zhao, G.: Magnetic ordered mesoporous copper ferrite as a heterogeneous Fenton catalyst for the degradation of imidacloprid. Appl. Catal. B-Environ. **147**, 534–545 (2014)
11. Albuquerque, A.S., Tolentino, M.V.C., Ardisson, J.D., Moura, F.C.C., de Mendonca, R., Macedo, W.A.A.: Nanostructured ferrites: Structural analysis and catalytic activity, Ceram. Int. 38, 2225–2231 (2012)
12. Jauhar, S., Singhal, S.: Substituted cobalt nano-ferrites, $CoMxFe_{2-x}O_4$ ($M=Cr^{3+}$, Ni^{2+}, Cu^{2+}, Zn^{2+}; $0.2 \le x \le 1.0$) as heterogeneous catalysts for modified Fenton′s reaction. Ceram. Int. **40**, 11845–11855 (2014)
13. Velinov, N., Petrova, T., Genova, I., Ivanov, I., Tsoncheva, T., Idakiev, V., Kunev, B., Mitov, I.: Synthesis and Mössbauer spectroscopic investigation of copper-manganese ferrite catalysts for water-gas shift reaction and methanol decomposition. Mater. Res. Bull. **95**, 556–562 (2017)
14. Gaikwad, P.V., Kamble, R.J., Mane-Gavade, S.J., Sabale, S.R., Kamble, P.D.: Magneto-structural properties and photocatalytic performance of sol-gel synthesized cobalt substituted NiCu ferrites for degradation of methylene blue under sunlight. Phys. B Condens. Matter. **554**, 79–85 (2019)

15. Shi, B., Zhang, Z., Zha, B., Liu, D.: Structure evolution of spinel Fe-MII (M=Mn, Fe, co, Ni) ferrite in CO hydrogenation. Mol. Catal. **456**, 31–37 (2018)
16. Sutka, A., Mezinskis, G.: Sol–gel auto-combustion synthesis of spinel-type ferrite nanomaterials. Front. Mater. Sci. **6**, 128–141 (2012)
17. Szczygieł, I., Winiarska, K.: Synthesis and characterization of manganese–zinc ferrite obtained by thermal decomposition from organic precursors. J. Therm. Anal. Calorim. **115**, 471–477 (2014)
18. Dhiman, M., Singhal, S.: Enhanced catalytic properties of rare-earth substituted cobalt ferrites fabricated by sol-gel auto-combustion route. Mater. Today Proc. **14**(2), 435–444 (2019)
19. Pei, J., Wang, Z., Gao, Y., Zhang, H.: Structure and magnetic properties of $Ni_{0.5}Zn_{0.5}Mn_{0.5-x}Mo_xFe_{1.5}O_4$ ferrites prepared by sol-gel auto-combustion method. Curr. App. Phys. **19**(4), 440–446 (2019)
20. Ateia, E.E., Soliman, F.S.: Multiferroic properties of Gd/Er doped chromium ferrite nano sized particles synthesized by citrate auto combustion method. Mater. Sci. Eng. B. **244**, 29–37 (2019)
21. Velinov, N., Petrova, T., Tsoncheva, T., Genova, I., Koleva, K., Kovacheva, D., Mitov I.: Auto-combustion synthesis, mössbauer study and catalytic properties of copper-manganese ferrites. Hyperfine Interact. 237 (1), art. no. 24, 1–11 (2016)
22. Koleva, K., Velinov, N., Tsoncheva, T., Mitov, I.: Mössbauer study of $Cu_{1-x}Zn_xFe_2O_4$ catalytic materials. Hyperfine Interact. **226**, 89–97 (2014)
23. Žák, T., Jirásková, Y.: CONFIT: Mössbauer spectra fitting program. Surf. Interface Anal. **38**, 710–714 (2006)
24. Ortega López Y., Medina Vázquez H., Salinas Gutiérrez J., Guzmán Velderrain V., López Ortiz A., Collins Martínez V.: Synthesis method effect of $CoFe_2O_4$ on its photocatalytic properties for H_2 production from water and visible light. J. Nanomater. 2015, Article ID 985872, 1–9 (2015)
25. Al-Ghamdi, A.A., Al-Hazmi, F.S., Memesh, L.S., Shokr, F.S., Bronstein, L.M.: Evolution of the structure, magnetic and optical properties of $Ni_{1-x}CuxFe_2O_4$ spinel ferrites prepared by soft mechanochemical method. J. Alloys Comp. **712**, 82–89 (2017)
26. Balavijayalakshmia, J., Suriyanarayanan, N., Jayaprakash, R.: Role of copper on structural, magnetic and dielectric properties of nickel ferrite nano particles. J. Magn. Magn. Mater. **385**, 302–307 (2015)
27. Huang, Y.-H., Wang, S.-F., Tsai, A.-P., Kameoka, S.: Catalysts prepared from copper-nickel ferrites for the steam reforming of methanol. J. Power Sources. **281**, 138–145 (2015)